JOURNAL OF APPLIED ELECTROCHEMISTRY 14 (1984) 769–777

The behaviour of a two-compartment stirred-tank electrochemical reactor with two anodic reactions and with continuous flows of both anolyte and catholyte

D. J. PICKETT, S. J. SUDALL

Department of Chemical Engineering, The University of Manchester Institute of Science and Technology, Manchester M60 1QD, UK

Received 14 November 1983; revised 17 February 1984

A partial mathematical model is presented for a two-compartment electrochemical reactor when there is a steady flow into and out of each compartment and when both anolyte and catholyte are well mixed. Two simultaneous anodic reactions, the fast oxidation of ferrocyanide ions and oxygen evolution, together with cathodic hydrogen evolution are considered and both migration and diffusion of hydroxyl ions across the diaphragm are taken into account. The resulting differential equations relate the concentrations of hydroxyl ions in each compartment and anolyte ferrocyanide to time in terms of, *inter alia*, the total reactor current and the partial current for ferrocyanide oxidation. By using the measured variation of current with time from an experimental reactor operated at a constant voltage and estimating the ferrocyanide partial current the observed concentration–time variations can be matched with those obtained by numerical integration of the model equations. Data from a series of experiments have been analysed and the assumption of a constant partial ferrocyanide current over the duration of a run gives a satisfactory representation of the behaviour of the experimental reactor. Reasons for discrepancies are discussed.

1. Introduction

A number of simple mathematical models for two-compartment electrochemical reactors with various operational modes have been presented by Pickett [1]. In a number of these models well-mixed conditions in both anode and cathode compartments were assumed and the occurrence of two anodic reactions, one of them fast and the other of oxygen evolution (slow) was considered. A single reaction (hydrogen evolution from an alkaline solution) was taken as the cathodic process.

In these models ionic transfer across the diaphragm was assumed to be due to migration only and, for some cases, the predicted variations of concentrations of reacting species with time were shown to be in qualitative accord with experimental data obtained by Sudall [2].

One mode of operation dealt with briefly but not subjected to comparison with experimental data was the case of steady flows into and out of both compartments. Sufficient detail was presented to show that the system operates at an unsteady state [1].

In this paper, this latter operational mode is re-examined and a partial model is developed that includes both migration and diffusion across the diaphragm. Further data by Sudall [2] are used to provide values for some of the parameters and to examine the applicability of the model for this system.

2. Reactor model

Fig. 1 illustrates the operational mode of the reactor. One feed, consisting of a solution of KOH and $K_4Fe(CN)_6$ flows to the anode compartment where the reactions

$$Fe(CN)_6^{4-} \longrightarrow Fe(CN)_6^{3-} + e \qquad (1)$$

and

0021–891X/84 $03.00 + .12

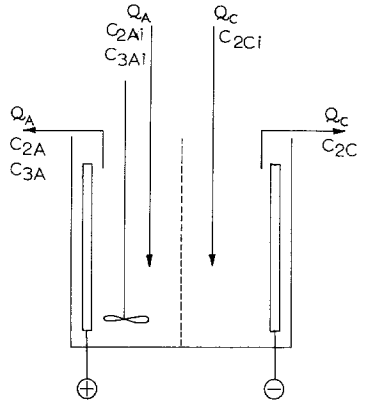

Fig. 1. Sketch of the reactor operational mode.

$$4OH^- \longrightarrow O_2 + 2H_2O + 4e \qquad (2)$$

take place. Mechanical stirring and the oxygen evolution ensure that the anolyte is well mixed so that the composition of the solution leaving the anode compartment is the same as that within it. The feed to the cathode compartment is a solution of potassium hydroxide. The only cathodic reaction is

$$2H_2O + 2e \longrightarrow H_2 + 2OH^- \qquad (3)$$

and it is assumed that the gas produces well-mixed catholyte having the same composition as solution leaving the cathode compartment. The following are the main additional assumptions:

(a) no volume changes take place due to decomposition and vaporization of water
(b) ionic transfer across the diaphragm occurs by migration and diffusion only
(c) no ferrocyanide and ferricyanide ions are transferred to the cathode compartment
(d) the reactor is operated at a total current I which may vary with time and which is greater than or equal to the partial current I_1 for ferrocyanide oxidation
(e) operation is isothermal

Any further assumptions will be noted when they are made.

For simplicity the following notation will be applied to the molar ionic concentrations: subscripts 1, 2, 3, 4 refer to K^+, OH^-, $Fe(CN)_6^{4-}$ and $Fe(CN)_6^{3-}$, respectively; subscripts C and A refer to catholyte and anolyte; i refers to feeds and o refers to initial conditions. Thus, as examples, C_{3Ai} is the concentration of ferrocyanide ions in the feed to the anode compartment and C_{2C} is the concentration of hydroxyl ions in the catholyte at any time t.

If the volumetric flow rate of anolyte feed is Q_A and the volume of the anolyte in the reactor is v_A then an instantaneous ferrocyanide material balance at time t is

$$Q_A C_{3Ai} = Q_A C_{3A} + v_A \frac{dC_{3A}}{dt} + \frac{I_1}{F} \qquad (4)$$

where F is the Faraday number.

Simultaneously, a hydroxyl ion balance over the anode compartment gives

$$Q_A C_{2Ai} = Q_A C_{2A} + N_2 A + \frac{(I - I_1)}{F} + v_A \frac{dC_{2A}}{dt} \qquad (5)$$

The second term on the right hand side of Equation 5 is the product of the hydroxyl ion flux across the diaphragm multiplied by the diaphragm area, A. N_2 will be positive if the transfer is from the anolyte to the catholyte. The third term in the equation is the rate of consumption of hydroxyl ions associated with the anodic evolution of oxygen.

A third material balance can be written for the hydroxyl ions on the cathode side. If v_C is the volume of catholyte and Q_C the flow rate then

$$Q_C C_{2Ci} = Q_C C_{2C} - \frac{I}{F} - N_2 A + v_C \frac{dC_{2C}}{dt} \qquad (6)$$

The above equations are subject to the initial conditions:

$$C_{2A} = C_{2Ao} \quad C_{3A} = C_{3Ao} \quad C_{2C} = C_{2Co} \quad \text{at } t = 0 \qquad (7)$$

The surfaces of the diaphragm are considered to be two parallel planes with one-dimensional ionic transfer taking place. The thickness of the diaphragm is δ with the anolyte/diaphragm interface located at $x = 0$ and the catholyte/diaphragm interface at $x = \delta$. If C_1, C_2, C_3, C_4 represent the concentrations of the relevant ionic species in the solution contained within the diaphragm then at the interfaces

$$C_1 = C_{1A} \quad C_2 = C_{2A} \quad C_3 = C_{3A} \quad C_4 = C_{4A} \quad \text{at } x = 0 \tag{8a}$$

$$C_1 = C_{1C} \quad C_2 = C_{2C} \quad C_3 = 0 \quad C_4 = 0 \quad \text{at } x = \delta \tag{8b}$$

The ionic fluxes within the diaphragm are assumed to be given by dilute solution theory, for example, Newman (see [3]) and, in the absence of flow, the instantaneous flux N_j of ionic species j is given by

$$N_j = -D_j \frac{dC_j}{dx} - U_j C_j z_j F \frac{d\phi}{dx} \tag{9}$$

In Equation 9 D_j is the diffusivity of j, U_j the ionic mobility, z_j the charge on j and ϕ the potential of the solution in the diaphragm. The ionic mobility and the diffusivity are related by the Nernst–Einstein equation

$$D_j = RTU_j \tag{10}$$

Noting that $N_3 = N_4 = 0$ from Assumption c above and also that $z_1 = 1, z_2 = -1, z_3 = -4$ and $z_4 = -3$ then successive applications of Equations 9, 10 give the individual fluxes as:

$$N_1 = -D_1 \frac{dC_1}{dx} - \frac{D_1 C_1 F}{RT} \frac{d\phi}{dx} \tag{11}$$

$$N_2 = -D_2 \frac{dC_2}{dx} + \frac{D_2 C_2 F}{RT} \frac{d\phi}{dx} \tag{12}$$

$$0 = -D_3 \frac{dC_3}{dx} + \frac{4D_3 C_3 F}{RT} \frac{d\phi}{dx} \tag{13}$$

$$0 = -D_4 \frac{dC_4}{dx} + \frac{3D_4 C_4 F}{RT} \frac{d\phi}{dx} \tag{14}$$

Since the solution is electrically neutral then at all points

$$C_1 - C_2 - 4C_3 - 3C_4 = 0 \tag{15}$$

Dividing each of Equations 11–14 by its respective diffusivity, summing and eliminating $d\phi/dx$ by means of Equation 15 gives

$$\frac{-d}{dx}[C_1 + C_2 + C_3 + C_4] = \frac{N_1}{D_1} + \frac{N_2}{D_2} \tag{16}$$

and a further application of Equation 15 to eliminate C_1 produces

$$\frac{-d}{dx}[2C_2 + 5C_3 + 4C_4] = \frac{N_1}{D_1} + \frac{N_2}{D_2} \tag{17}$$

Equation 17 can be integrated across the diaphragm using the boundary conditions given in Equation 8a, b resulting in

$$2(C_{2C} - C_{2A}) - 5C_{3A} - 4C_{4A} = \left[\frac{N_1}{D_1} + \frac{N_2}{D_2}\right]\delta \tag{18}$$

A more general form of Equation 18 takes into account the possible presence of ferricyanide ions in the anolyte feed and also the fact that the combined concentrations of ferrocyanide and ferricyanide are constant in the anolyte.

$$C_T = C_{3Ai} + C_{4Ai} \tag{19}$$

$$= C_{3A} + C_{4A} \tag{19a}$$

Equation 19a can be used to eliminate C_{4A} from Equation 18.

$$2(C_{2C} - C_{2A}) - 4C_T - C_{3A} = \left[\frac{N_1}{D_1} + \frac{N_2}{D_2}\right]\delta \tag{20}$$

The potassium and hydroxyl ion fluxes through the diaphragm N_1 and N_2 can also be equated to the total reactor current by

$$I = AF(N_1 - N_2) \tag{21}$$

Eliminating N_1 between Equations 20 and 21 and rearranging gives the following equation for the hydroxyl ion flux:

$$N_2 = \frac{D_1 D_2}{D_1 + D_2}\left[\frac{2(C_{2C} - C_{2A}) - 4C_T - C_{3A}}{\delta} - \frac{I}{AFD_1}\right] \tag{22}$$

It may be noted that a simpler model in which only migration of OH^- is considered would be represented by the last term only in the above equation and this corresponds to

$$N_2 = -\left[\frac{D_2}{D_1 + D_2}\right]\frac{I}{AF} \tag{23}$$

the term in brackets being the transport number of hydroxyl ions in a KOH solution.

Equation 22 is used in Equations 5 and 6 to eliminate N_2 and the resulting equations, together

with Equation 4, can be rearranged to give the rates of change of concentration with time, namely,

$$\frac{dC_{3A}}{dt} = \frac{Q_A}{v_A}[C_{3Ai} - C_{3A}] + \frac{I_1}{v_A F} \quad (24)$$

$$\frac{dC_{2A}}{dt} = \frac{Q_A}{v_A} C_{2Ai} + \frac{1}{v_A}\left[\frac{2D_1D_2A}{(D_1+D_2)\delta} - Q_A\right]C_{2A} - \frac{I}{v_A F}\left[\frac{D_1}{D_1+D_2}\right] + \frac{I_1}{v_A F} - \frac{D_1D_2A}{v_A(D_1+D_2)} \times \frac{2C_{2C} - 4C_T - C_{3A}}{\delta} \quad (25)$$

$$\frac{dC_{2C}}{dt} = \frac{Q_C}{v_C} C_{2Ci} - \frac{1}{v_C}\left[\frac{2D_1D_2A}{(D_1+D_2)\delta} + Q_C\right]C_{2C} + \frac{I}{v_C F}\left[\frac{D_1}{D_1+D_2}\right] - \frac{2D_1D_2A}{v_C(D_1+D_2)} \times \frac{2C_{2A} + 4C_T + C_{3A}}{\delta} \quad (26)$$

Equations 24–26 are applicable if the ferrocyanide reaction alone takes place at the anode in which case $I = I_1$ in the above equations. The general case represents operation above the limiting current for ferrocyanide oxidation although it is not possible to give an explicit relationship for I_1. The limiting current will be enhanced due to the stirring effect of evolved gas and will depend on the partial current $(I - I_1)$ in addition to its dependence on Q_A, v_A, C_{3A} and the rate of mechanical stirring.

In no practical cases can I_1 (I_L) be explicitly related to the above parameters, nor can the reactor current be predicted under constant voltage operation. Consequently, 'predicted' concentration–time relationships by integration of Equations 24–26 can only be obtained using measured I vs t data available from constant voltage experiments and estimating the magnitude of I_1. The most convenient choice for I_1, notwithstanding the comments above, is to assume that it is constant for the duration of a run. These factors mean that the model has to be applied in an interpretive or semi-theoretical manner.

The constant value assigned to I_1 permits the current efficiency for the oxidation of ferrocyanide ions, ϵ, under constant voltage operation to be given by

$$\epsilon = \frac{I_1 \tau}{\int_0^\tau I dt} \quad (27)$$

where τ is the operating time.

The remaining unassigned parameters in the model equations are D_1 and D_2 which are obtained from published data on KOH solutions. These values are multiplied by the porosity of the diaphragm to give a truer expression of the fluxes through the porous structure.

3. Experimental details

A side view of the electrochemical reactor is shown in Fig. 2. It consisted of two compartments separated by a cylindrical diaphragm. The reaction vessel was a glass cylinder 12 in tall and 11.5 in i.d. the ends of which fitted into grooves machined in perspex end plates. The end plates were $\frac{3}{4}$ in thick and 16 in diameter, the bottom one being supported on a $\frac{1}{4}$ in thick mild steel plate. Compression was effected by eight 5/16 in diameter mild steel tie rods and a seal achieved by two 1/16 in thick neoprene gaskets. The anode and cathode consisted of two concentric rings of nickel mesh, 94 and 178 mm diameter, respectively each 206 mm long. The mesh size was 25 x 25 count with 0.375 mm wire size and 0.125 mm wire thickness. The meshes were strengthened by perspex rings at the bottom and nickel current distribution rings at the top, and positioned with respect to the vessel and diaphragm by means of perspex spacers. The diaphragm was a Celloton H125 grade ceramic cylinder supplied by Doulton Industrial products. The mean i.d. was 149 mm and mean wall thickness 9.9 mm and the maximum pore size was 1 μm. One end of the diaphragm was closed and this was inlaid into the bottom end plate. A neoprene gasket fitted between the open lip of the diaphragm and the top end plate to prevent gas mixing. The anode compartment was equipped with a centrally located four bladed 50 mm diameter stainless steel paddle stirrer. The stirrer shaft passed through a stirrer gland in the top perspex plate. The shaft was connected to a variable speed electric motor by means of an electrically insulated flexible drive.

Electrical power was supplied using a Harmsworth a.c. to d.c. conversion unit (0–8 V

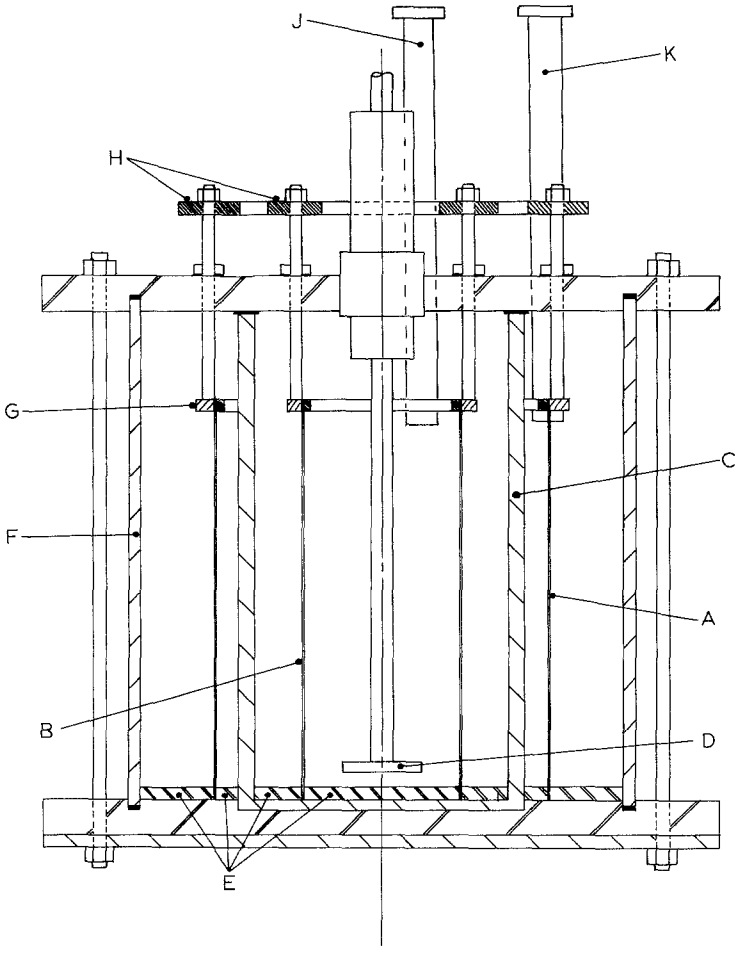

Fig. 2. The experimental reactor: A = nickel mesh cathode, B = nickel mesh anode, C = porous pot diaphragm, D = stainless steel paddle, E = mesh spacer/supports, F = glass vessel, G = current distribution rings, H = copper contact plates, J = anolyte inlet tube, K = catholyte inlet tube.

and 0–70 A). The applied voltage and electrode potentials were measured using a Pye electronic voltmeter and the current measured with a Model 8 Mark IV Avometer together with 25 A and 100 A shunts as appropriate. The electrode potential probes were conventional Luggin capillaries referenced to saturated calomel electrodes. One probe per electrode was employed and both could be located at any vertical position. A conventional flow circuit was used for the anolyte, consisting of a 24 litre stainless steel reservoir, pump, rotameters, constant head tank and a spent anolyte receiver. The anolyte level was controlled by applying a vacuum from a water pump to the outlet flow line which was at the same level as that in the reactor. The anolyte temperature was regulated when necessary by using a small stainless steel heat exchanger in the upstream part of the flow circuit. In order to prevent decomposition of ferricyanide by light all glass surfaces except the reactor vessel were covered with black adhesive tape. Flow of catholyte was from a head tank, the circuit being simpler than for the anolyte since a constant flow rate was used. An identical level control to the one on the anode side was set up. Samples of both anolyte and catholyte were obtained directly from the reactor by means of a pipette.

Typical anolyte compositions were 0.3–0.5 mol dm^{-3} $K_4Fe(CN)_6$ and 0–0.3 mol dm^{-3} KOH (SLR grades). However, the anolyte collected from a run was used as the feed for the next run providing the ferrocyanide concentration was acceptably high. The catholyte was a solution of potassium hydroxide in the range 0.3–1.1 mol dm^{-3} KOH. A run commenced by setting both anolyte and catholyte flow rates and recirculating until inlet and outlet temperatures were equal. Stirring of the anolyte was then begun and a constant e.m.f. applied to the reactor. Measure-

ments of flow rates, total current, stirrer speed and electrode potentials were made at set time intervals along with sampling of anolyte and catholyte. The duration of a run was $1\frac{1}{2}$–2 h and was mainly influenced by the anolyte flow rate. The amounts of ferrocyanide and ferricyanide present in the anolyte samples were determined by a spectrophotometric procedure developed by Sudall [2]. Hydroxyl ion concentrations were determined by titration with standard acid. Full experimental details are available in the reference by Sudall [2].

4. Results and discussion

4.1. *Solution of model equations*

Integration of the concentration–time Equations 24–26 for given flow rates, Q_A, Q_C, inlet concentrations, C_{3Ai}, C_{2Ai}, C_{2Ci}, initial concentrations, C_{3Co}, C_{2Ao}, C_{2Co} and total current, I, requires values for the parameters v_A, v_C, δ, D_1, D_2, together with an estimate for the partial current, I_1. The following values were used in all calculations.

anolyte volume, v_A (m^3)	$= 3.616 \times 10^{-3}$
catholyte volume, v_C (m^3)	$= 1.052 \times 10^{-2}$
mean diaphragm thickness, δ (mm)	$= 9.9$
mean diaphragm area, A (m^2)	$= 0.968$
diffusivity of K^+ (D_1) in the diaphragm ($m^2\ s^{-1}$)	$= 8.665 \times 10^{-10}$
diffusivity of OH^- (D_2) in the diaphragm ($m^2\ s^{-1}$)	$= 2.328 \times 10^{-9}$

The diffusivities are estimated values at 20° C based on KOH diffusivity data [4] and anion transport numbers [5] in the approximate range 0–1 mol dm^{-3} multipled by a factor of 0.50 which is the diaphragm porosity. The logarithmic mean diaphragm area has been used since the model has been set up in a one-dimensional form.

Under constant voltage operation, the total current varies with time as typified by Fig. 3. Since the variation is gradual, linear interpolation between successive measurements was adopted to provide I as a function of t. As discussed previously, I_1 is taken to have a constant value over the duration of a run except for a few cases when only ferrocyanide oxidation occurred. Then, I_1 is described by the I vs t relationship determined above. In those instances where oxygen evolution did not take place at the start of a run, I_1 was also described by the I vs t data until the estimated I_1 became equal to the measured value of I (the start of the second reaction).

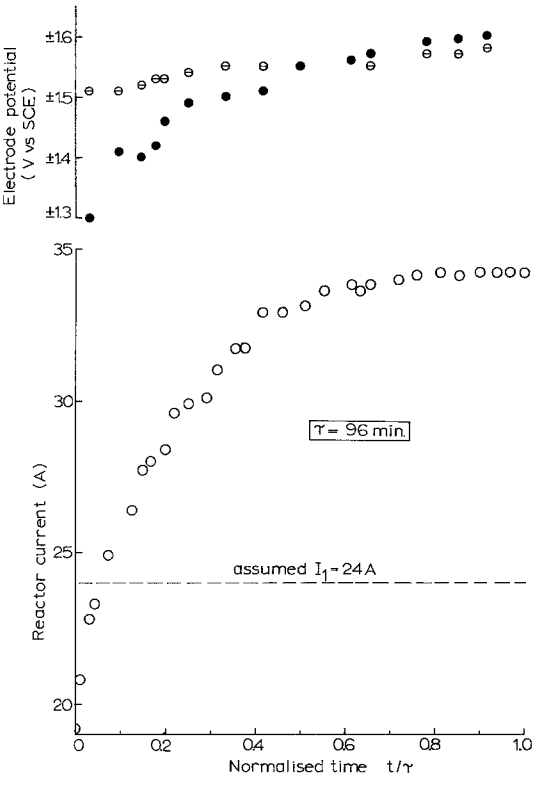

Fig. 3. Variation of electrode potentials and total reactor current with time for run 1: ⊖ – cathodic, ● – anodic.

With I_1 assigned in the manner described and all necessary parameters initialized, Equations 24–26 were integrated simultaneously using a fourth order Runge–Kutta procedure. Computed final concentrations were compared with experimental values and the procedure repeated for new values of I_1 until satisfactory agreement was obtained. No explicit criteria were used to define the best fit of data, cognisance of the general correspondence between experiment and prediction over a run being taken into account. Additionally, computation of the total quality of electricity passed during a run was made and the current efficiency for ferrocyanide oxidation obtained by evaluating Equation 27.

Table 1. Experimental data and model predictions

Run	1	2	3	4	5	6	7	8	9	10
Applied e.m.f. (*V*)	4.0	4.0	4.5	5.0	3.0	3.0	3.5	5.0	4.0	5.0
Stirrer r.p.m.	0	0	400	400	650	650	1300	1300	1300	1300
Q_A ($dm^3\ h^{-1}$)	8.82	12.00	15.50	6.63	15.50	15.50	6.65	6.63	12.00	6.90
Q_C ($dm^3\ h^{-1}$)	9.00	9.00	9.00	9.00	9.00	9.00	9.00	9.00	9.00	9.00
Assumed I_1 (*A*)	24.0	30.0	54.5	24.0	29.0	35.0	27.0	19.0	14.0	62.0
Initial concentrations ($mol\ dm^{-3}$)										
C_{3Ao}	0.437	0.346	0.300	0.256	0.461	0.504	0.207	0.143	0.077	0.456
C_{2Ao}	0.000	0.029	0.087	0.072	0.001	0.046	0.106	0.064	0.092	0.000
C_{2Ao}	0.594	0.310	1.156	0.320	0.681	0.672	1.087	0.324	0.611	0.377
Inlet concentrations ($mol\ dm^{-3}$)										
C_{3Ai}	0.437	0.346	0.304	0.248	0.461	0.364	0.207	0.142	0.077	0.456
C_{2Ai}	0.000	0.029	0.086	0.072	0.001	0.044	0.106	0.064	0.092	0.000
C_{2Ci}	0.594	0.310	1.156	0.320	0.681	0.672	1.087	0.324	0.611	0.377
Final concentrations ($mol\ dm^{-3}$)										
C_{3A} predicted	0.338	0.256	0.174	0.122	0.391	0.299	0.060	0.041	0.033	0.137
C_{3A} actual	0.336	0.247	0.171	0.118	0.393	0.281	0.061	0.041	0.035	0.133
C_{2A} predicted	0.059	0.090	0.180	0.125	0.050	0.090	0.204	0.098	0.109	0.220
C_{2A} actual	0.058	0.073	0.156	0.105	0.067	0.094	0.198	0.092	0.098	0.207
C_{2C} predicted	0.622	0.337	1.201	0.360	0.707	0.694	1.117	0.362	0.631	0.436
C_{2C} actual	0.632	0.367	1.197	0.357	0.713	0.697	1.136	0.361	0.631	0.394
τ (*min*)	96	80	93	88	106	77	119	96	63	102
$\int_0^\tau Idt(kC)$	171	149	302	240	173	115	243	246	112	383
Predicted current efficiency	0.76	0.94	0.98	0.53	1.00	1.00	0.79	0.44	0.47	0.99

4.2. *Comparison of experimental data and model predictions*

Table 1 presents experimental data for ten runs and includes the predicted final concentrations. In addition, Figs. 4–6 show all experimental and computed concentration–time data for Runs 1, 5 and 9, respectively. All three graphs show that the reactor tends to approach quasi-steady conditions under quite widely varied anolyte flow rates, stirrer speeds, applied e.m.f.s and inlet concentrations. These plots are also representative of the other tabulated runs.

Data from Run 1 are also presented in Figs. 3 and 7. Fig. 3 gives the experimental variations of electrode potentials and total current with time and Fig.7 presents the variations in anolyte and catholyte temperatures. Fig. 7 will be discussed later.

In Run 1 no mechanical stirring was used so that anolyte mixing was due solely to flow and oxygen evolution. The poorer mixing is revealed in Fig. 4 where very significant discrepancies between measured and predicted anolyte hydroxyl ion concentrations are shown. The assumed value of 24 A used for I_1 in the computation for Fig. 4 has been superimposed on the current–time plot in Fig. 3 and the progressive rise in the oxygen partial current with time is visible. This suggests that the mixing in the anode compartment will be improved with time and this fact is to a reasonable extent substantiated by closer agreement between measured and predicted C_{3A} and C_{2A} for $t > 0.6\tau$ plotted in Fig. 4.

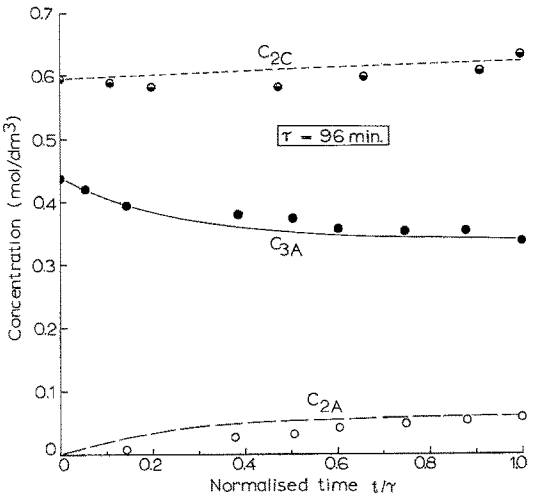

Fig. 4. Comparison of experimental and predicted concentration–time curves for Run 1.

In Run 5 oxygen evolution does not take place and the reactor operates throughout under sub-limiting current conditions (Fig. 5). The higher anolyte flow rate and the use of mechanical stirring compared with Run 1 produces marginally better mixing.

On the cathode side of the reactor agreement between measured and predicted hydroxyl ion concentrations in Runs 1 and 5 is judged to be satisfactory. Some non-uniformity in concentration is almost certainly due to the large catholyte volume despite the stirring effect of the

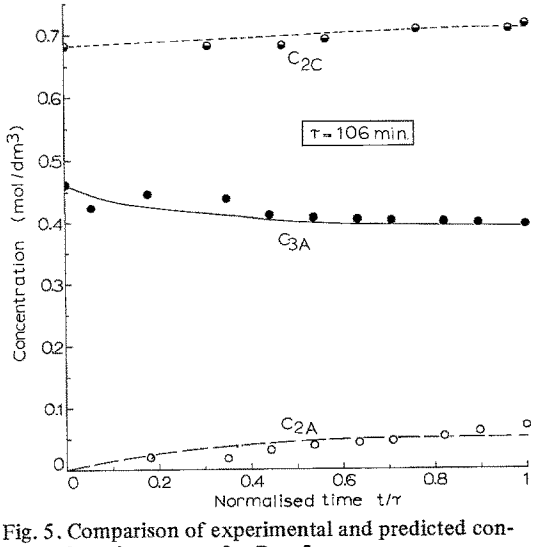

Fig. 5. Comparison of experimental and predicted concentration–time curves for Run 5.

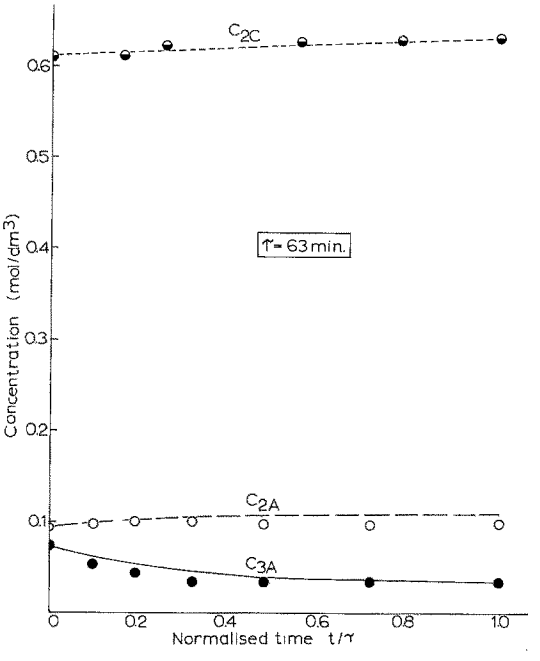

Fig. 6. Comparison of experimental and predicted concentration–time curves for Run 9.

evolved hydrogen. In general measured hydroxyl ion concentrations in the catholyte are lower than those predicted and this suggests the existence of a small bulk flow of dilute alkali from the anode compartment, even though no ferrocyanide or ferricyanide was detected in the catholyte. Negligible concentration changes occur due to the decomposition of, and vaporization of water and in any event such effects would cause increase in measured concentrations. Examination of the variations of electrode potentials with time presented in Fig. 3 is instructive. Since the reactor

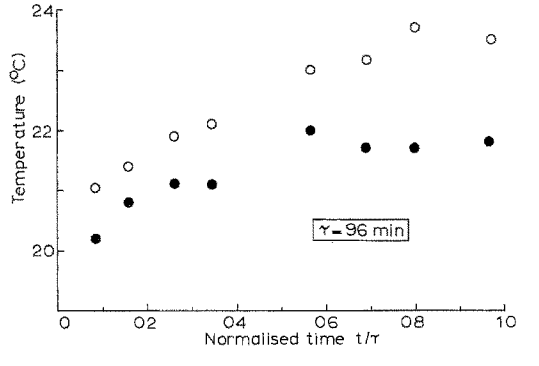

Fig. 7. Variations of anolyte and catholyte temperatures with time for Run 1 • – anolyte, ○ – catholyte.

is operated at a constant voltage with a continuous rise in the conductivities of both anolyte and catholyte, the increase in the magnitudes of both potentials with time is expected. The rise in cathode potential is small and gradual whereas the anode potential increases much more rapidly in the initial stages. The latter phenomenon is due to the change in surface conditions produced by oxygen evolution. In those runs where oxygen evolution either did not occur or occurred at a small partial current the anode potential increased only slightly with time.

The temperature–time variations for catholyte and anolyte plotted as given in Fig. 7 also show gradual temperature increases over a run and approach steady-state. The catholyte temperature is approximately 1–1.5° C greater than that of the anolyte and this was observed in all experiments. In view of the much smaller anolyte volume it can be concluded that the cathodic reaction is taking place under significantly more irreversible conditions than either or both of the anodic reactions. Despite the changes of and differences in temperatures, the assumption of isothermal conditions is satisfactory, with negligible errors introduced by taking ionic diffusivity values at 20° C.

The concentration–time data for Run 9 (Fig. 6) correspond to the lowest ferrocyanide inlet concentration used in the ten runs and the shortest operation time. In this case the secondary anodic reaction occurred at an appreciable rate throughout. Satisfactory correspondence between measured and predicted concentrations is apparent, however the actual anolyte composition became substantially constant after about 0.3τ. A probable reason for the discrepancy in ferrocyanide concentrations below 0.3τ is the assumption of a constant value of I_1 in the computation. Initially I_1 would be higher than predicted because of its proportionality to the instantaneous ferrocyanide concentration. Thus the latter would decrease more rapidly with time than predicted by the model. The same, of course, could be said of Run 1, but the effect is much more pronounced in Run 9 where the greater stirrer speed and oxygen partial current give much improved mass transfer to the anode surface.

Insufficient data prohibits the evaluation of a quantitative relationship for the mass transfer coefficient at the anode as a function of the flow rate, stirrer speed and oxygen partial current. Examination of I_1 and C_{3A} measured values given in Table 1 does show some trends. In particular Runs 1 and 2 show an increase with flow rate when no stirring was used and comparison between Runs 8, 9 and 10 show that the effect of stirrer speed is very much greater than that of the gas evolution. This is not surprising since flow is *through* the mesh electrode rather than over it, the latter state being more commonly used in reactor studies.

A few final remarks are useful about the general applicability of this type of electrochemical reactor. This paper refers to comparatively short operating times following a start-up but it is important to recognize that the system is inherently an unsteady-state over any operating interval. In the present study the reactant concentrations are seen to come to quasi-steady values but this may not be general.

5. Conclusions

The partial model developed for a two-compartment stirred tank electrochemical reactor with separate anolyte and catholyte feeds and two anodic reactions has been shown to give a good quantitative description of the performance of an experimental reactor by using an estimated partial current for the main anodic reaction in the model equations. The largest discrepancies have been seen to be due to poor mixing, uncertainty in the prediction of the partial current at low reactant concentrations and the probable existence of a small bulk flow from anode to cathode compartment.

References

[1] D. J. Pickett, 'Electrochemical Reactor Design', 2nd ed., Elsevier, Amsterdam (1979).
[2] S. J. Sudall, PhD thesis, University of Manchester (1975).
[3] J. S. Newman, 'Electrochemical Systems', Prentice Hall, Englewood Cliffs, New Jersey (1973).
[4] H. R. Bruins, 'International Critical Tables. Vol. 5', McGraw-Hill, New York (1929) p. 68.
[5] D. Dobos, 'Electrochemical Data', Elsevier, Amsterdam (1975).